Available online at www.sciencedirect.com

ScienceDirect

Advances in Space Research 72 (2023) 2860–2873

ADVANCES IN SPACE RESEARCH (a COSPAR publication)

www.elsevier.com/locate/asr

Autonomous obstacle avoidance strategies in the mission of large space debris removal using potential function

Chuangge Wang, Danhe Chen *, Wenhe Liao, Zhenhua Liang

School of Mechanical Engineering, Nanjing University of Science and Technology, Nanjing 210094, China

Received 2 January 2022; received in revised form 15 March 2022; accepted 6 April 2022
Available online 11 April 2022

Abstract

Debris removal problem has become a consensus of international communities with the dramatically increase of space debris. When the service spacecraft (Servicer) carries out debris removal operations, there may exist collision threaten from other small objects which fly around the target debris. In this paper, autonomous collision avoidance strategies using improved potential function are studied, which drive the Servicer to rendezvous with the large debris and avoid obstacles around the trajectory. Firstly, the repulsive potential for static obstacles is constructed based on the relative position vector. Considering the necessary of avoidance of dynamic obstacles, the relative velocity vector between the Servicer and dynamic obstacles in space is introduced to design the repulsive potential for dynamic obstacles. Also, the corresponding control law is derived to drive the Servicer to approach the large debris. Finally, numerical simulations are performed to validate the effectiveness and stability of the obstacle avoidance strategy for debris removal.

Keywords: Debris removal; Collision avoidance; Potential function; Static obstacles; Dynamic obstacles

1. Introduction

More than 27,000 pieces of space debris are tracked by the Department of Defense's global Space Surveillance Network (SSN) sensors. The population of space debris is still rising with the frequent space activities of human beings, which increases the potential danger to all spacecrafts in space, especially in the International Space Station (Mark and Kamath, 2019; Liou, 2011). Nearly 50% of space debris is generated by the explosive disintegration or collision of satellites, which are the main sources of space debris (Liou, 2008). There are several prominent debris addition events which have been recorded in recent history, such as the collision of Kosmos 2251 and Iridium 33 in 2009 and explosive disintegration of U.S. DMSP-F13 satellite in 2015 (Kessler et al., 2010; Pang et al., 2015). Recently, Russia carried out an antisatellite test and destroy one of its own satellite Kosmos-1408 on 2021 November the 15th, which produced at least 1500 pieces of trackable debris (Valencia and Eng, 2021). It is imperative to develop the guidelines and carry out the space missions of large debris removal to purify the space environment for the spacecraft safety in future.

Large quantities of space debris generated by explosion disintegration or collision will evolve into debris cloud (Letizia et al., 2016; Salnikova et al., 2020). As different types and sizes debris are mixed together, large space debris often surrounded by plenty of small debris. The applicable safety distance of most debris removal systems is within tens of meters (Nanjangud et al., 2018), such as net (Shan et al., 2020), harpoon (Aglietti et al., 2020; Forshaw et al., 2020), electric tether (Nishida et al., 2009) and solid rocket de-orbiting (Naumann et al. 2019). The Servicer needs to maneuver within this range of the large space debris and then there will be a risk of collision with

* Corresponding author.
E-mail address: cranefeeling@hotmail.com (D. Chen).

https://doi.org/10.1016/j.asr.2022.04.013
0273-1177/

other small debris. Thus, it is necessary to avoid other space debris using obstacle avoidance method when the Servicer maneuvers to the target debris (Hu et al., 2021).

The artificial potential function method was initially used for the path planning of robot (Khatib, 1986; Patle et al., 2019), and it was later applied to the guidance and control of spacecraft by Lopez and Mclnnes (1995). As a virtual force method, potential function has a simple structure and strong adaptability, which is suitable for real-time maneuver control and collision avoidance of spacecraft and has been used in several typical space missions. Jiang et al. (2021) combined the interfered fluid dynamical system and potential function to solve the problem of obstacle avoidance in the process of spacecraft rendezvous. Badawy and McInnes (2008) proposed a super-quadric potential function for the autonomous on-orbit assembly of a large space structure and collision avoidance can make use of both translational and rotation maneuvers to reduce total maneuver cost. Yang et al. (2022) solved formation reconstruction problem for multi-spacecrafts with collision avoidance using potential field approach. Roger and McInnes (2000) used Laplace artificial potential function to construct the actual shape of the International Space Station and planned the flying path around it. Yu et al. (2021) proposed a distributed autonomous low-thrust control method incorporating with the potential function to solve the cluster gathering problem. Then Monte Carlo analysis demonstrated the effectiveness of this method. By combining the sliding mode technique with the potential function, Li et al. (2018) presents a robust adaptive control strategy for driving the chaser spacecraft to rendezvous and dock with a space target without violating the path constraint. In the asteroid landing and sample return missions, Zhu et al. (2022) designed a new repulsive potential function in logarithmic form, which effectively avoided the spacecraft falling into local minimum zone in complex terrains.

Recently, the potential function has been integrated with other methods to achieve widely application. Munoz (2011) introduced dynamics into the potential function, and solved the problem of optimal control with collision avoidance. Cao et al. (2018) has designed a new improved potential function based on sliding mode control for the guidance and control of spacecraft rendezvous considering the obstacles avoidance, which can guarantee the value of potential function converge to zero at the desired state. In addition, for tracking of moving targets, Friudenberg and Koziol (2018) combined potential function with parallel navigation to achieve rendezvous of moving targets and avoid obstacles. Choi et al. (2021) proposed an intelligent cooperative collision avoidance approach combining the potential field with a fuzzy inference system and provide a near optimal collision-free trajectory. In summary, there are many researches on collision avoidance using potential function, but most studies assume the obstacles are static. However, many scenarios of future debris removal for large debris will involve dynamic obstacles. Although there is some research on the collision avoidance of robots against dynamic obstacles (Ge and Cui, 2002), the application in space is still facing challenges. Considering the constraints of external disturbance and thrust limitation, the problem of approaching target and avoiding static and dynamic obstacles in complicated space environment deserves further investigation.

Motivated by the foregoing discussions, this paper aims at developing autonomous obstacle avoidance strategies when approaching the target in the mission of large debris removal. Main contributions of this paper are summarized as follows:(1) the potential function for dynamic obstacles is constructed and the relative velocity vector between the Servicer and the obstacles is introduced into the repulsive function. (2) The control law combining repulsive potential of the static and dynamic obstacles is designed based on the gradient of repulsive function. (3) The simulation in complicated scenario is carried out to verify the adaptability of the avoidance strategy for static and dynamic obstacles in space.

The rest of this paper is organized as follows. In Section 2, the problem formulation is given including the mission introduction, relevant coordinate frames, dynamics equation. Two potential functions are established in Section 3, including potential function for static obstacles and dynamic obstacles, and the control law is proposed. Also, the local minimum problem of potential function is discussed, and escape force is introduced to solve the problem of local minimum. In Section 4, the numerical simulation of three scenarios are carried out, and the simulation results are presented and analyzed. The conclusions are provided in Section 5.

2. Problem formulation

2.1. Mission introduction

The removal of large space debris is a complicated space mission, the process scheme including phasing maneuvering, autonomous collision avoidance etc, as shown in Fig. 1. After launched into orbit, the Servicer is far from the target debris and it will take a long time to approach the target debris through phasing maneuvering (Zhang et al., 2015), and the Servicer avoids collisions mainly through the prediction of ground station at this time (Sun et al. 2020). Then the Servicer enters the close range of maneuver, applying closed-loop feedback control method to approach the target via relative navigation. More importantly, there may exists debris around the target, the Servicer needs to maneuver flexibly to avoid those possible collisions. Depending on the relative velocity of debris around the target, it can be regarded as static and dynamic obstacle. Therefore, in the final rendezvous phase an autonomous obstacle avoidance strategy of the Servicer should be developed.

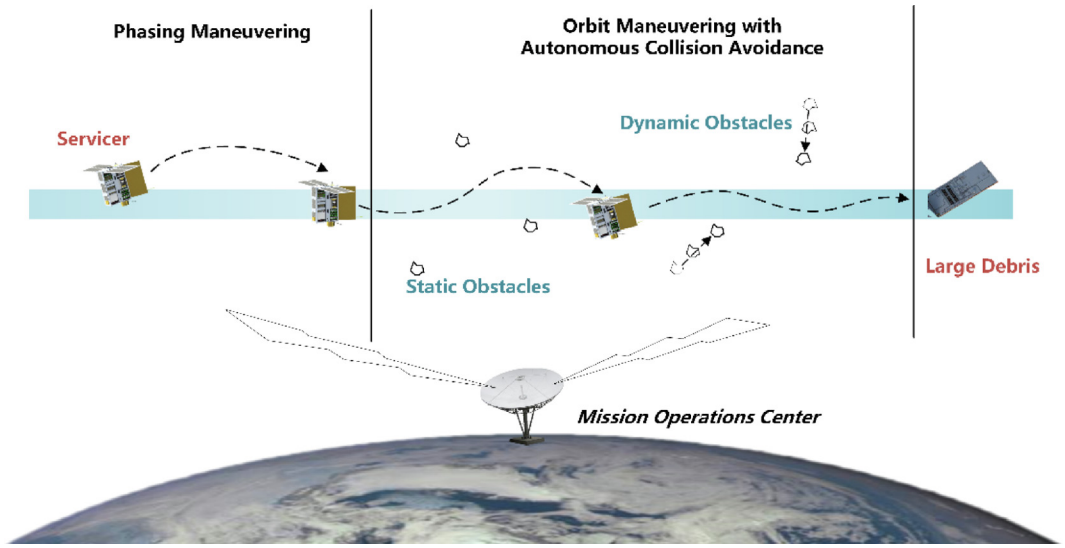

Fig. 1. Debris removal process.

2.2. Relative dynamic model

The coordinate reference frames (LVLH coordinate) used here are shown in Fig. 2, which is defined as follows: Earth-centered inertial coordinate system $OXYZ$ has its origin O located in the mass center of the Earth. The X axis points toward the vernal equinox. The Z axis is along the north pole, and the Y axis completes the triad. The target orbit coordinate system has its origin located in the center of mass of the target. The x-axis points from the center of earth to the mass center of the Servicer. The y axis is perpendicular to $\times$ axis in the target orbital plane and is positive along the flight direction. The z axis is located in the normal direction of the target orbit.

To directly describe the relative position between the Servicer and target, the orbital dynamics of the relative motion are established in the LVLH coordinate system. The dynamics equation of the Servicer relative to the target is derived as (Van der Ha and Mugellesi, 1990).

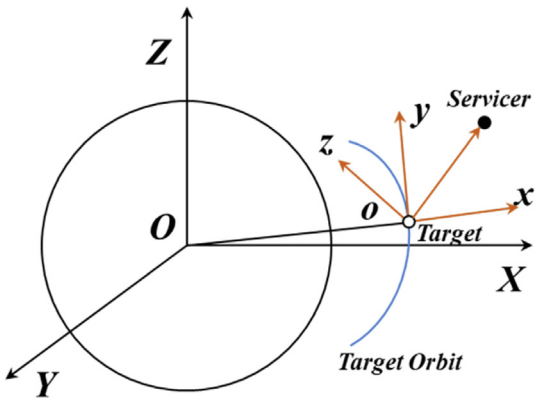

Fig. 2. Target LVLH Coordinate Frame.

$$\begin{cases} \ddot{x} = \dot{\theta}^2 x + \ddot{\theta} y + 2\dot{\theta}\dot{y} + 2\frac{\mu x}{r_t^3} + f_{dx} + u_x \\ \ddot{y} = -\ddot{\theta} x + \dot{\theta}^2 y - 2\dot{\theta}\dot{x} - \frac{\mu y}{r_t^3} + f_{dy} + u_y \\ \ddot{z} = -\frac{\mu z}{r_t^3} + f_{dz} + u_z \end{cases} \tag{1}$$

where, μ is the gravitational constant of the earth; $\mathbf{x} = [x\, y\, z]^T$ is the position of the Servicer; $\boldsymbol{f}_d = [f_{dx} f_{dy} f_{dz}]^T$ is the perturbation acceleration; $\boldsymbol{u} = [u_x\, u_y\, u_z]^T$ is the control acceleration on the Servicer; θ is the true anomaly. If the target moves in a circular orbit, i.e. $e = 0$, $\dot{\theta}$, $\ddot{\theta}$ can be written as $\dot{\theta} = n$, $\ddot{\theta} = 0$, where n is mean angular velocity of the target orbit and Eq. (1) is transformed into the Hill–Clohessy–Wiltshire (HCW) equation.

3. Obstacle avoidance strategies

In this section, potential function is applied to avoid obstacles in the rendezvous process of space debris. Two kinds of potential function are proposed to avoid the possible collisions, which are used for static and dynamic obstacles respectively. Then, the control law based on the gradient of the proposed potential function are designed for the close-range approach.

3.1. Artificial potential function

The artificial potential function adopts the idea of potential to establish a virtual potential field around obstacle and target. The target is located at the lowest point of the virtual potential field, and the potential field around obstacle is convex. Driven by the gradient of potential field, the controlled spacecraft moves from higher potential position to lower in order to avoid obstacles. As shown in Fig. 3, the potential field is established on a two-

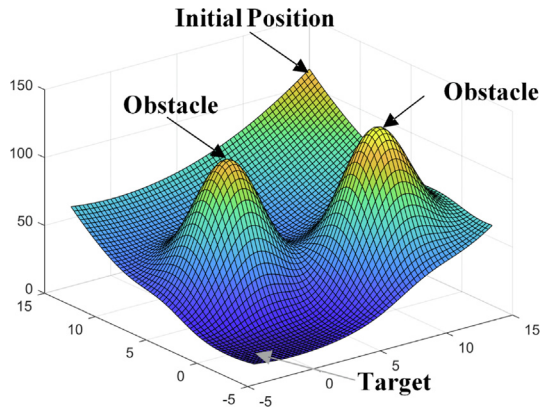

Fig. 3. Artificial Potential Field.

dimensional plane. Suppose an object is in its initial position and is expected to reach its target. The object will autonomously move towards the position of the lowest potential energy, where the target locates. At the same time, due to the convex area around obstacle, the object will actively avoid obstacle to achieve collision avoidance.

The artificial potential function method is composed of attractive and repulsive potentials, which are utilized to derive the necessary control inputs to reach the target. The attraction potential function establishes a global minimum value at the goal position driving the Servicer to the target. The repulsive potential function establishes a region of high potential field at the location of obstacle, which generates repulsive force to drive away the Servicer. The total potential function, ϕ_t, is defined as the superposition of attractive potentials and the sum of repulsive potential in the workspace,

$$\phi_t = \phi_a + \sum_{i=1}^{N} \phi_{r_i} \tag{2}$$

where N is the number of obstacles; ϕ_a is the attractive potential and ϕ_{r_i} is the i-th repulsive potential.

Since the space environment is complex, all the space debris cannot be considered relatively static. In this paper, artificial potential functions for static obstacles and dynamic obstacles are designed separately.

3.2. Potential function for static obstacles

As stated in Eq. (2), the total potential consists of attractive potential and repulsive potential, where ϕ_a is the attractive potential, defined by a quadratic function.

$$\phi_a = \frac{k_a}{2}(\boldsymbol{x_s} - \boldsymbol{x_t})^T \boldsymbol{Q}_a (\boldsymbol{x_s} - \boldsymbol{x_t}) \tag{3}$$

where k_a is a positive constant; $\boldsymbol{Q}_a$ is the symmetric, positive definite, attractive potential shaping matrix; $\boldsymbol{x_s} = [x_s, y_s, z_s]^T$ represents the Servicer state and $\boldsymbol{x_t} = [x_t, y_t, z_t]^T$ represents the goal state. ϕ_{r_i} is the repulsive potential of i-th obstacle and is defined as.

$$\phi_{r_i} = \frac{(\boldsymbol{x_s} - \boldsymbol{x_t})^T \boldsymbol{Q}_{o_i} (\boldsymbol{x_s} - \boldsymbol{x_t})}{2\left((\boldsymbol{x_s} - \boldsymbol{x}_{o_i})^T \boldsymbol{P}_{o_i} (\boldsymbol{x_s} - \boldsymbol{x}_{o_i}) - d_r\right)} \; i = 1, 2, \cdots, m \tag{4}$$

where $\boldsymbol{Q}_{o_i}$ and $\boldsymbol{P}_{o_i}$ are the symmetric, positive matrices that define the shape of repulsive potential, respectively; d_r is a positive constant; m is the number of static obstacles. From a geometric perspective, the shaping matrix $\boldsymbol{Q}_o$ affects the height of the potential field while $\boldsymbol{P}_o$ and d_r affect the width of potential field. These three parameters are selected to ensure that the resulting repulsive potential field encompasses the whole of a static obstacle, such as a Servicer that cannot collide with an obstacle.

In the far-field, the attraction of attractive potential acts primarily on the Servicer, attracting it to maneuver to the target position. When the Servicer approaches the obstacle, the repulsive force of obstacle plays a major role, keeping the Servicer away from the obstacle. The corresponding virtual force is defined as the negative gradient of the potential in terms of position. The gradient of attractive and repulsive potential function is.

$$\nabla_x \phi_a = k_a \boldsymbol{Q_a} \boldsymbol{r}_{st} \tag{5}$$

$$\nabla_x \phi_{r_i} = \frac{\left(\boldsymbol{r}_{so_i}^T \boldsymbol{P}_{o_i} \boldsymbol{r}_{so_i} - d_r\right) \boldsymbol{Q}_{o_i} \boldsymbol{r}_{st} - \boldsymbol{r}_{st}^T \boldsymbol{Q}_{o_i} \boldsymbol{r}_{st} \boldsymbol{P}_{o_i} \boldsymbol{r}_{so_i}}{\left(\boldsymbol{r}_{so_i}^T \boldsymbol{P}_{o_i} \boldsymbol{r}_{so_i} - d_r\right)^2} \tag{6}$$

where $\boldsymbol{r}_{st}$ is the relative position of the Servicer with respect to the target position; $\boldsymbol{r}_{so_i}$ is the relative position of the Servicer with respect to the i-th obstacle.

Thus, the repulsive force generated by the i-th static obstacle is.

$$\boldsymbol{u}_{reps_i} = -\nabla_x \phi_{r_i} \tag{7}$$

3.3. Potential function for dynamic obstacles

The potential function for static obstacles has been designed in the last section, in which only the relative position is considered. For the dynamic obstacles, the relative velocity between Servicer and the obstacle should be introduced into the potential function (Ge and Cui, 2002) (Mancini et al., 2019).

The relative velocity between Servicer and obstacle in the direction of the Servicer pointing to the obstacle is described as.

$$v_{so_j}(t) = [\boldsymbol{v_s} - \boldsymbol{v}_{o_j}]^T \boldsymbol{n}_{so_j} = [\boldsymbol{v_s} - \boldsymbol{v}_{o_j}]^T \frac{\boldsymbol{x}_{o_j} - \boldsymbol{x_s}}{\|\boldsymbol{x}_{o_j} - \boldsymbol{x_s}\|} \tag{8}$$

where, $\boldsymbol{v_s}$ is the velocity of Servicer; $\boldsymbol{v}_{o_j}$ is the velocity of j-th obstacle; $\boldsymbol{n}_{so_j}$ is the unit vector pointing from Servicer to the j-th obstacle. If $v_{so_j}(t) > 0$, i.e. the Servicer is moving close to the dynamic obstacle, avoidance maneuver would be implemented. If $v_{so_j}(t) \leq 0$, that is Servicer is moving away from the dynamic obstacle, and Servicer does not need to avoid these dynamic obstacles.

As the Servicer is moving toward obstacle with relative velocity $v_{so_j}(t)$, it should keep a shortest safety distance

d_m to the obstacle and in which the Servicer can be decelerated before collision with obstacle. If a maximum deceleration of magnitude a_{max} is applied to the Servicer to reduce its velocity, distance d_m of the Servicer moving before v_{so_j} reduces to zero can be approximated as.

$$d_m(v_{so_j}) = \frac{v_{so_j}^2(t)}{2a_{max}} \tag{9}$$

Then, the relative velocity is converted into relative distance. The repulsive potential for dynamic obstacles is defined as follows:

$$\phi_{d_j} = \eta\left(\frac{1}{d_s(\boldsymbol{x_s} - \boldsymbol{x}_{o_j}) - d_m(v_{so_j})} - \frac{1}{d_0}\right) \tag{10}$$

where, ϕ_{d_j} denotes the repulsive potential generated by the j-th dynamic obstacle; $d_s(\boldsymbol{x_s} - \boldsymbol{x}_{o_j})$ represents the distance between Servicer and the j-th obstacle; d_0 is a positive constant describing the influence range of obstacle; η is a positive constant.

According to Eq. (8), the gradients of $\boldsymbol{v_{so_j}}(t)$ with respect to both velocity and position are given respectively as.

$$\nabla_{\boldsymbol{v}}\boldsymbol{v_{so_j}}(t) = \boldsymbol{n}_{so_j} \tag{11}$$

$$\nabla_{\boldsymbol{x}}\boldsymbol{v_{so_j}}(t) = \frac{[v_{so_j}(t)\boldsymbol{n}_{so_j} - (\boldsymbol{v_s} - \boldsymbol{v}_{o_j})]}{\|\boldsymbol{x_s} - \boldsymbol{x}_{o_j}\|} \tag{12}$$

Then, we can obtain the gradients of repulsive potential for the j-th dynamic obstacle in terms of position and velocity.

$$\nabla_v\phi_{d_j} = \eta\frac{1}{\left(d_s(\boldsymbol{x_s} - \boldsymbol{x_{so_j}}) - d_m(v_{so_j})\right)^2}\left(1 + \frac{v_{so_j}}{u_{max}}\right)\boldsymbol{n_{so_j}} \tag{13}$$

$$\nabla_x\phi_{d_j} = \eta\frac{-v_{so_j}v_{so_j\perp}}{d_s(\boldsymbol{x_s} - \boldsymbol{x_{so_j}})a_{max}\left(d_s(\boldsymbol{x_s} - \boldsymbol{x_{so_j}}) - d_m(v_{so_j})\right)^2}\boldsymbol{n_{so_j\perp}} \tag{14}$$

where,

$$v_{so_j\perp} = \sqrt{\|\boldsymbol{v_s} - \boldsymbol{v_{o_j}}\|^2 - {v_{so_j}}^2} \tag{15}$$

Thus, the repulsive force generated by the j-th obstacle is.

$$\boldsymbol{u}_{repd_j} = \begin{cases} 0, if d_s(\boldsymbol{x_s} - \boldsymbol{x_{so_j}}) - d_m(v_{so_j}) \geq d_0 or v_{so_j} \leq 0 \\ \boldsymbol{u_{rep_{j1}}} + \boldsymbol{u_{rep_{j2}}} if d_s(\boldsymbol{x_s} - \boldsymbol{x_{so_j}}) - d_m(v_{so_j}) < d_0 and v_{so_j} > 0 \end{cases} \tag{16}$$

where $\boldsymbol{u_{rep_{j1}}} = -\nabla_x\phi_{d_j}$; $\boldsymbol{u_{rep_{j2}}} = -\nabla_v\phi_{d_j}$.

The relationship between the repulsive force components is shown in the Fig. 4. The repulsive force $\boldsymbol{u_{rep_{j1}}}$ points to Servicer from the obstacle, driving the spacecraft far away from the obstacle. The repulsive force $\boldsymbol{u_{rep_{j2}}}$ is oriented perpendicular to $\boldsymbol{u_{rep_{j1}}}$, driving the spacecraft bypass the obstacle. $\boldsymbol{u_{rep_{j2}}}$ is perpendicular to $\boldsymbol{u_{rep_{j1}}}$ and coplanar with $\boldsymbol{u_{rep_{j1}}}$ and $\boldsymbol{v_{so_j}}$.

In the real space mission, there will be a safe distance between spacecraft and obstacle, i.e., the nearest distance d_{safe} between spacecraft and obstacle, and it is introduced into the repulsive potential function to adjust the safe distance in practical application. For different obstacles, various safe distances can be defined to reduce the further risk of collision. Thus, the repulsive potential can be modified slightly as follows:

$$\phi_{r_j} = \eta\left(\frac{1}{d_s(\boldsymbol{x_s} - \boldsymbol{x_{so_j}}) - d_{safe} - d_m(v_{sO_i})} - \frac{1}{d_0}\right) \tag{17}$$

3.4. Control law

The control law is critical in the process of collision avoidance, it can be designed based on the gradient of attractive and repulsive potential field. Considering that there are both static obstacles and dynamic obstacles in space near spacecraft, then the real time control low of the Servicer can be defined as.

$$\boldsymbol{u_s} = -k(k_a\boldsymbol{Q_a}\boldsymbol{r}_{st} - (\dot{\boldsymbol{x}}_t - \dot{\boldsymbol{x}}_s)) + k_s\sum_{i=1}^{m}\boldsymbol{u}_{reps_i} + k_d\sum_{j=1}^{n}\boldsymbol{u}_{repd_j} \tag{18}$$

where k, k_s, k_d are positive constants representing the weights of attractive force, repulsive force of static obstacle and dynamic obstacle; m is the number of static obstacles; n is the number of dynamic obstacles. If the target is relatively static, Eq. (18) can be simplified as.

$$\boldsymbol{u_s} = -k(k_a\boldsymbol{Q_a}\boldsymbol{r}_{st} + \dot{\boldsymbol{x}}_s) + k_s\sum_{i=1}^{m}\boldsymbol{u}_{reps_i} + k_d\sum_{j=1}^{n}\boldsymbol{u}_{repd_j} \tag{19}$$

In practice, thruster saturation is ubiquitous. The real control signal is denoted by $\boldsymbol{u_{rs}} = [u_{rs_1}, u_{rs_2}, u_{rs_3}]^T$ for a vector $\boldsymbol{u_s} = [u_{s_1}, u_{s_2}, u_{s_3}]^T$, and.

$$u_{rs_i} = \begin{cases} u_{s_i}, |u_{s_i}| \leq u_{max} \\ u_{max}sign(u_{s_i}), |u_{s_i}| > u_{max} \end{cases} \tag{20}$$

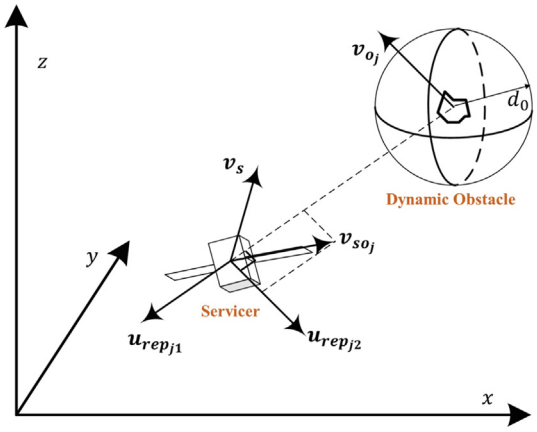

Fig. 4. Repulsive Force formed by Dynamic Obstacle.

where u_{max} denotes the maximum value of thrust acceleration; $sign(\cdot)$ denotes the standard signum operator; $i = 1, 2, 3$ represents the three directions of the coordinate system.

3.5. Problem of local minimum

The local minimum is a general problem to be tackled in the application of artificial potential function method. When the Servicer maneuvers along the gradient of the potential field may oscillate at the local minimum, the potential function we adopted also suffers from the local minimum. To solve the problem, the simplest method is to keep the Servicer moving according to the total control force as usual or waiting for the obstacles to change their motion. In this way, the Servicer will deviate from the local minimum.

In this paper, an escape force to avoid the local minimum (Prahlad et al., 2000) is introduced. In the potential field, local minimum exist near the null-potential points:

$$\boldsymbol{u}_a + \boldsymbol{u}_{rep} = 0 \tag{21}$$

where, $\boldsymbol{u}_a = -k_a \boldsymbol{Q}_a \boldsymbol{r}_{st}$ represents the attractive force; $\boldsymbol{u}_{rep} = \sum_{i=1}^{m} \boldsymbol{u}_{reps_i} + k_d \sum_{j=1}^{n} \boldsymbol{u}_{repd_j}$ represents the repulsive force.

A local minimum area is defined according to the following two conditions.

$$\left| \frac{\|\boldsymbol{u}_a\| - \|\boldsymbol{u}_{rep}\|}{\|\boldsymbol{u}_{rep}\|} \right| < l_a \tag{22}$$

$$\frac{\boldsymbol{u}_a \boldsymbol{u}_{rep}}{\|\boldsymbol{u}_a\| \|\boldsymbol{u}_{rep}\|} < -l_b \tag{23}$$

where, l_a and l_b are positive constants, and usually $l_a \in (0, 0.2)$, $l_a \in (0.8, 1)$. When the Servicer trap in a local minimum, an escape force $\boldsymbol{u}_e$ instead of control force $\boldsymbol{u}_s$ is applied:

$$\boldsymbol{u}_e = \boldsymbol{u}_{rep} \frac{\boldsymbol{u}_a \boldsymbol{u}_{rep}}{\|\boldsymbol{u}_a\| \|\boldsymbol{u}_{rep}\|} \tag{24}$$

Thus, driven by the escape force, the Servicer will leave the local minimum range.

4. Numerical simulation

In this section, the numerical simulation is carried out to verify the performance of the proposed method. Three simulation scenarios are considered formulated by two types of potential function. Here, we design a safe distance of 10 m for obstacles.

The geostationary orbit is valuable but there are also lots of space debris. It is crucial to remove space debris in this region to protect orbital resources. It is assumed that the large space debris to be removed is in geostationary orbit at an altitude of 35786 km. Furthermore, we adopt the thruster parameters in the CPOD mission for simulation, which weighs 6 kg and is equipped with a cool gas propulsion system, and the maximum thrust of satellite is $50mN$ (Bowen et al. 2015). The perturbation is represented by sinusoidal curve in numerical simulation (Pongvthithum et al., 2005), and the perturbation force is expressed as.

$$\boldsymbol{f}_d = \begin{bmatrix} \sin(\omega_0 t) & 0 & 0 \\ 0 & -\sin(\omega_0 t) & 0 \\ 0 & 0 & -\sin(\omega_0 t) \end{bmatrix} \bar{\boldsymbol{f}}_d \tag{21}$$

where, $\bar{\boldsymbol{f}}_d = [1.2 \quad 2.0 \quad 1.6]^T \times 10^{-5} m/s^2$; $\omega_0 = \sqrt{\mu/a^3}$ is the mean angular velocity of the target space debris.

The Servicer can be equipped by visual navigation system and LIDAR to obtain the real-time states of the obstacles (Roberto and Alessia, 2019) (Omri and Pini, 2021). If a special case occurs, the Servicer can't get the real-time state of dynamic obstacles, it can predict the state of dynamic obstacles through Kalman filter according to the initial measurement data (Prevost et al., 2007). Also, the state of dynamic obstacles can also be obtained by propagating in the relative dynamic model from its initial parameters. Therefore, it is assumed that the real-time state of dynamic obstacles is known to the Servicer simulation scenarios. At the same time, a random measurement error is introduced in the simulation to verify the robustness of the proposed algorithm.

4.1. Static obstacle avoidance

In this scenario (Scenario I), the proposed potential function for static obstacles in Section 3.2 is applied. The Servicer approaches the target debris from a long distance (1 km) to 100 m and avoids relatively static debris. The initial position of Servicer is $x_{s_0} = [0, -1000, 0]^T$ and the terminal position is $x_{s_t} = [0, -100, 0]^T$. In order to verify the availability of designed potential function, five obstacles are set in space, locate as $[0, -900, -10]^T$,

Table 1
Parameters in Scenario I.

Parameters	Symbol	Value
Matrix representing the magnitude of attractive potential	$\boldsymbol{Q}_a$	diag(0.004,0.004,0.004)
Matrix representing the magnitude of repulsive potential	$\boldsymbol{Q}_{Oi}$	diag(5,5,5)
Matrix representing the range of repulsive potential	$\boldsymbol{P}_{Oi}$	diag(1,1,1)
The influence distance of repulsive potential	d_r	100
The weights of attractive force	k	1
The positive gain of attractive potential	k_a	1
the weights of repulsive force of static obstacle	k_s	1

$[10, -760, 100]^T$, $[-50, -600, 120]^T$, $[0, -400, -100]^T$, $[0, -200, 35]^T$. Here, we assume the real-time state vector of obstacles is known to the Servicer and introduce a random measurement error of 3 m in three-axis to the simulation. These obstacles are located around the maneuvering trajectory of the Servicer and will threaten the Servicer. There will be collision risk if the Servicer approaches the goal point without the collision avoidance strategy. The simulation parameters set in scenario I are shown in Table 1.

The total simulation time is set as 1500 s, and the simulation step is 0.1 s. The simulation results are displayed in Fig. 5, which shows that the Servicer flexibly avoid all the five obstacle and is able to maneuver to the target debris. Fig. 5(b) plots the distance variation between the Servicer and each obstacle in the whole process. The closest distance between the Servicer and the five obstacles is 53.5 m, 105.5 m, 128.2 m, 145.1 m and 66.8 m, respectively, which reveals that the distance between the Servicer and the obstacles is greater than the safe distance of 10 m. Fig. 5

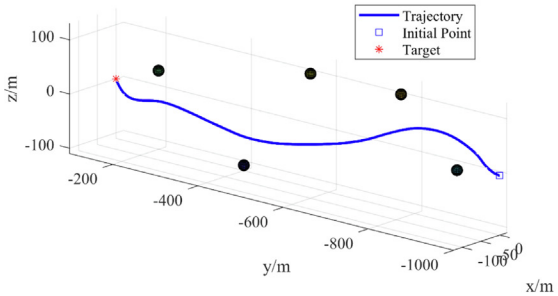

(a) Trajectory of the Servicer

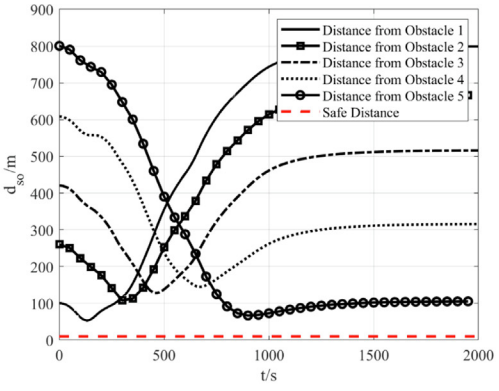

(b) Distance between the Servicer and obstacles

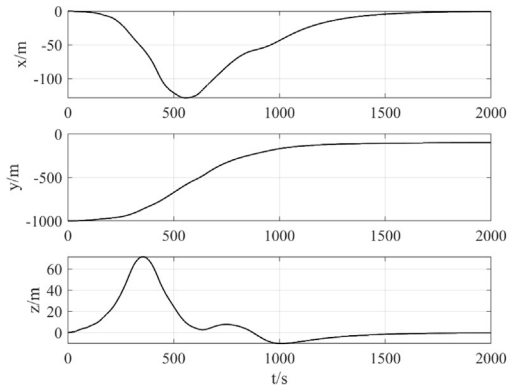

(c) Position of the Servicer

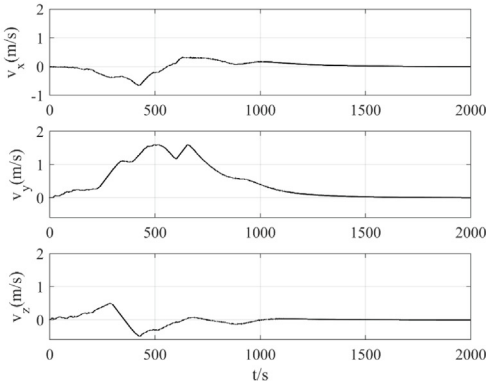

(d) Velocity of the Servicer

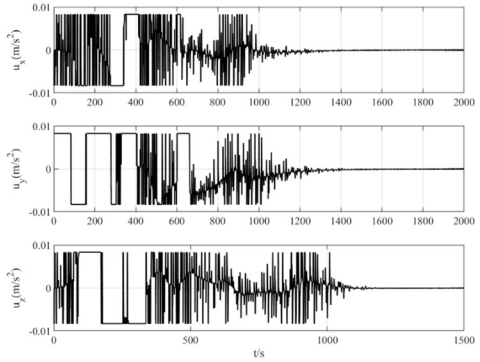

(d) Control acceleration of the Servicer

Fig. 5. Simulation results in Scenario I.

(c) and Fig. 5(d) display the Servicer's position and velocity. The Servicer's position converges to $[0,-100,0]^T$ and velocity converges to 0 under the proposed control law. The control acceleration is shown in Fig. 5d, which meets the thrust constraint and converges to 0 under the measurement error.

Moreover, the trajectories of the Servicer from different origins are displayed in Fig. 6 and the distance between these trajectories and obstacles is all greater than the safe distance. All the trajectories avoid the obstacles and reach the target, which indicates the strong robustness of this method.

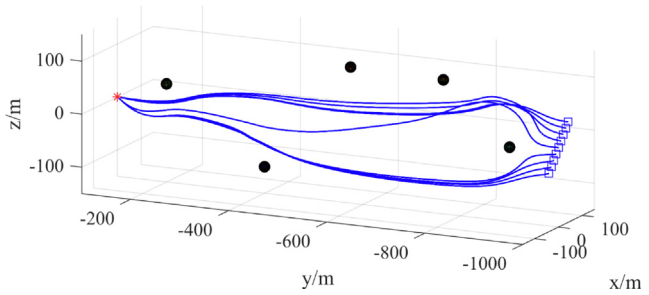

Fig. 6. The Trajectories of the Servicer from different initial points.

Table 2
Dynamic obstacle motion parameters.

Obstacle i	x_{O_0}(m)	v_{O_i}(m/s)
1	$[-10,-70,-10]^T$	$[0.14,\ -0.14,\ 0.14]^T$
2	$[-20,-50,\ 0]^T$	$[0.18,\ 0,\ 0]^T$
3	$[5,-21,-40]^T$	$[0,\ -0.05,\ 0.23]^T$

4.2. Dynamic obstacle avoidance

In this scenario (Scenario II), potential function for dynamic obstacles is adopted to avoid collision with obstacles and approach the target from 100 m to 10 m and the proposed potential function control law is compared with the SMC-APF control law in Reference (Mancini et al., 2020).

In the target orbit coordinate system, three dynamic obstacles are designed, and the target debris to be cleared is located at the origin of coordinates. The initial sate of the three debris are shown in Table 2 and their motion obeys the relative dynamic equation of the Eq. (1). The real-time state of the dynamic obstacles is known to the Servicer and introduce a measurement error of 3 m in three-axis.

The initial position of the Servicer is $\boldsymbol{x}_{s_0} = [0,-100,0]^T$ and the target point is origin of the orbital coordinate system. The simulation parameters of the proposed potential function control law for Scenario II are shown in Table 3. As for the SMC-APF control law in Reference (Mancini et al., 2020), the same values of $\boldsymbol{Q}_a$, k, k_a are used for the corresponding control gains. The control gains for the repulsive force in the SMC-APF are set as $k_{r,i} = 200$.

A preliminary simulation is carried out to verify that collisions would occur without collision avoidance control. As shown in Fig. 7, the sphere presents the no-fly zone

Table 3
Parameters in Scenario II.

Parameters	Symbol	Value
Matrix representing the magnitude of attractive potential function	$\boldsymbol{Q}_a$	diag(0.03,0.015,0.02)
The weights of attractive force	k	0.5
The positive gain of attractive potential	k_a	1
The weights of repulsive force of dynamic obstacle	k_d	1
The positive gain of repulsive potential	η	0.2

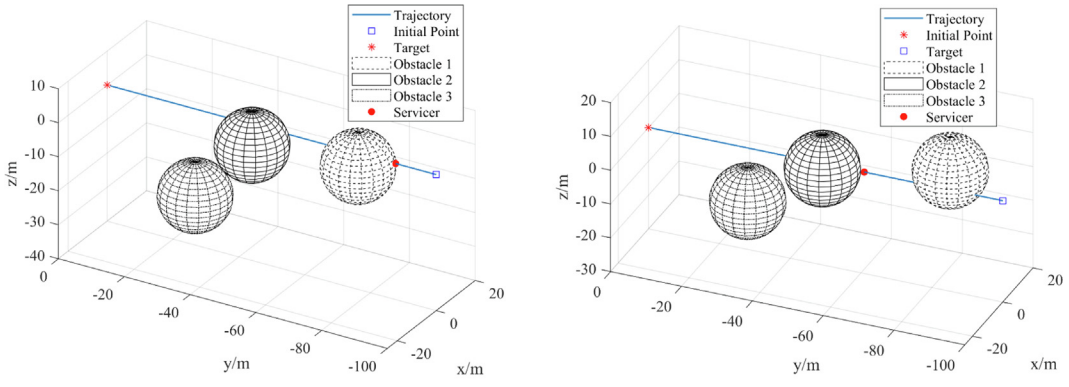

(a) Collision with Obstacle 1 at t=55s (b) Collision with Obstacle 2 at t=98s

Fig. 7. Simulation results in Scenario II without collision avoidance control.

around the obstacle. If there is only attractive force applied, the Servicer would approach the target in an approximate straight line and would collide with Obstacle 1 and Obstacle 2.

The simulation results with collision avoidance control are displayed in Fig. 8. Fig. 8(a) plots trajectories of the Servicer and the three dynamic obstacles under both control laws. Fig. 8(b) depicts the distance between the Servicer and obstacles. The closest distances to the three obstacles are 13.5 m, 18.6 m and 16.7 m for the proposed control law, and they are 10.8 m, 15.9 m, 16.4 m for the SMC-APF control law. It suggests that the proposed control law avoids the obstacles at a longer distance and improves safety. The motion of the Servicer is shown in Fig. 8(c). Both control laws can avoid dynamic obstacles, driving the Servicer to the target. The velocity of the Servicer is depicted in Fig. 8(d), which converge to 0 under both control laws. The three components of the velocity under the proposed control law are different from those under the SMC-APF control law. Moreover, the maximum

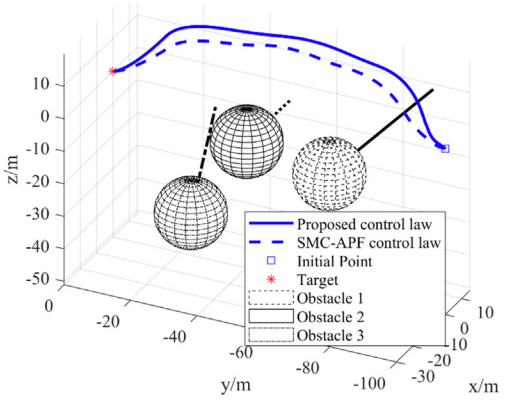

(a) Trajectory of the Servicer and obstacles

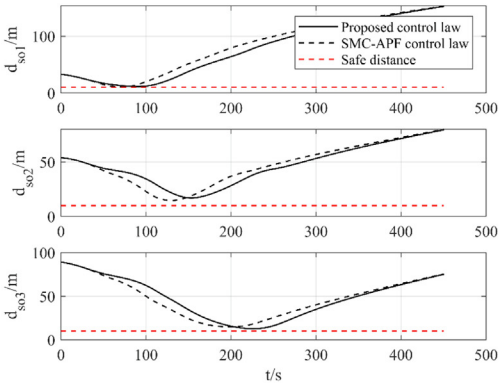

(b) Distance between the Servicer and three obstacles

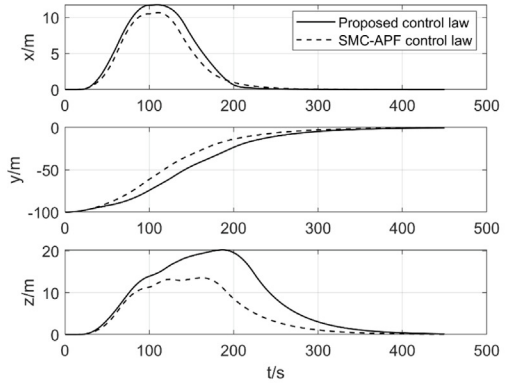

(c) Position of the Servicer

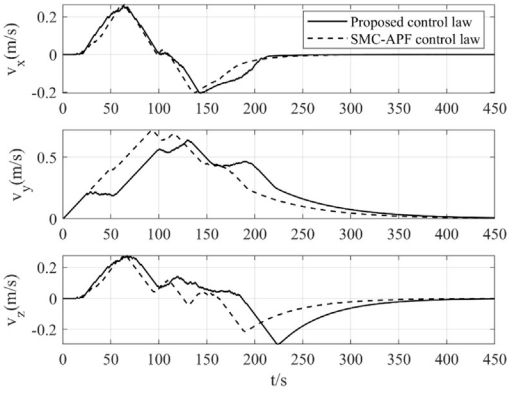

(d) Velocity of the Servicer

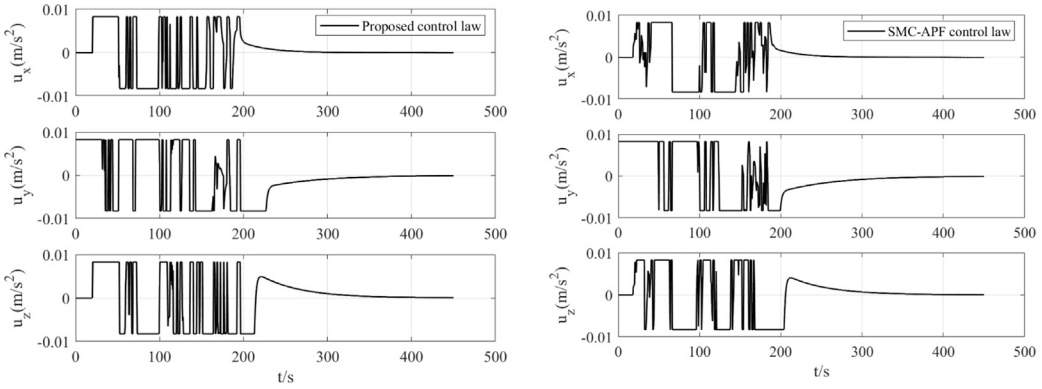

(e) Control acceleration of the Servicer

Fig. 8. Simulation results in Scenario II.

velocity of y axis in the SMC-APF control law is greater than that of the proposed control law, which is not conducive to the flexible control of the Servicer. The control acceleration in the LVLH frame is shown in Fig. 8(e), which converge to 0 under both control laws.

The trajectory of the Servicer at t = 60 s, t = 75 s, t = 125 s, t = 250 s are displayed in Fig. 9 under both control lows. Fig. 9(a) and Fig. 9(b) present the motion of the Servicer to avoid dynamic Obstacle 1 which shows that the trajectory of the Servicer turns significantly near the initial point. This is caused by the Servicer's avoidance to the dynamic Obstacle 1. Compared with the SMC-APF control law, the proposed control law enables the Servicer to keep a longer distance from Obstacle 1. Similarly, the avoidance trajectories of the Servicer towards Obstacles 2 and 3 are shown in Fig. 9(c) and 9(d). In three-dimensional space, there are more directions that can be maneuvered to avoid obstacles than in the plane, so the turning of obstacle avoidance path is not sharp and relatively gentle. Based on the above simulation results, the effectiveness of the potential function for dynamic obstacle avoidance can be proved.

4.3. Collision avoidance in compound space environment

In the previous section, we have simulated scenarios with single types of obstacles, respectively. But there may also exist relatively static and relatively dynamic obstacles simultaneously in some compound space environments, which are different from the above two scenarios. Here, we conduct simulation in this compound scenario and adopt the proposed potential function to verify the performance of the method. Three dynamic obstacles and three static obstacles are set in this compound scenario. The parameters of the three dynamic obstacles are the same as described in Section 4.2. The location of the three static obstacles is $[15, -71, -12]^T m$, $[-15, -30, 20]^T m$, $[10, -20, -20]^T m$. It is assumed that the relative state of dynamic and static obstacles is known to the Servicer and a random measurement error of 3 m is introduced into the simulation in three-axis. The control law of the Servicer is defined as Equation 1. The parameter settings are shown in Table 4.

Simulation results are displayed in Fig. 10. It can also be found in the Fig. 10(a) that the trajectory of the spacecraft has been obviously changed compared with the simulation

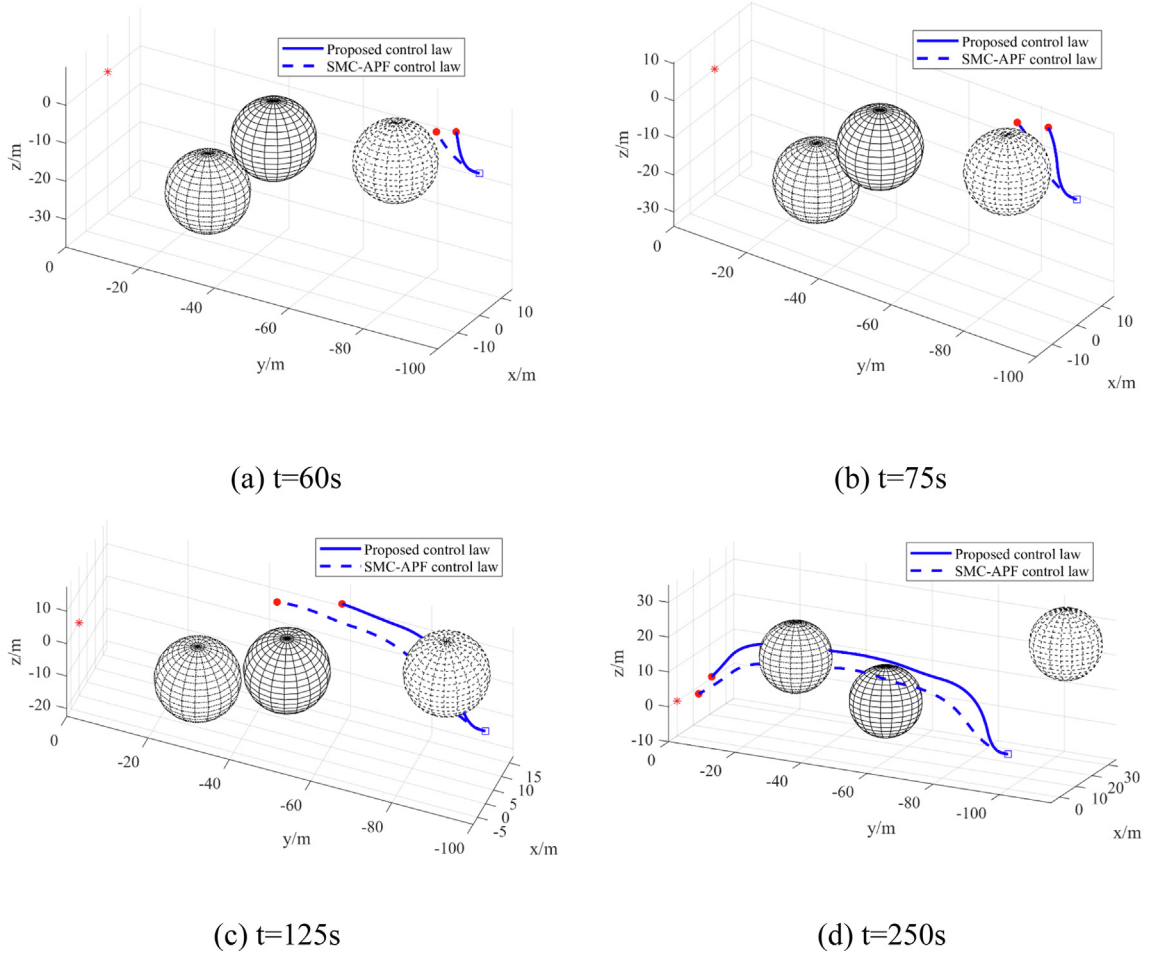

Fig. 9. Trajectory of the Servicer at (a)t = 60 s, (b)t = 75 s, (c)t = 125 s, (d)t = 250 s.

Table 4
Parameters in Scenario III.

Parameters	Symbol	Value
Matrix representing the magnitude of attractive potential function	Q_a	diag(0.02,0.02,0.01)
Matrix representing the magnitude of repulsive potential function	Q_{Oi}	diag(10,10,10)
Matrix representing the range of repulsive potential function	P_{Oi}	diag(5,5,5)
The weights of attractive force	k	0.1
The positive gain of attractive potential	k_a	1
The weights of repulsive force of static obstacle	k_s	1
The weights of repulsive force of dynamic obstacle	k_d	1
The positive gain of repulsive potential	η	0.1

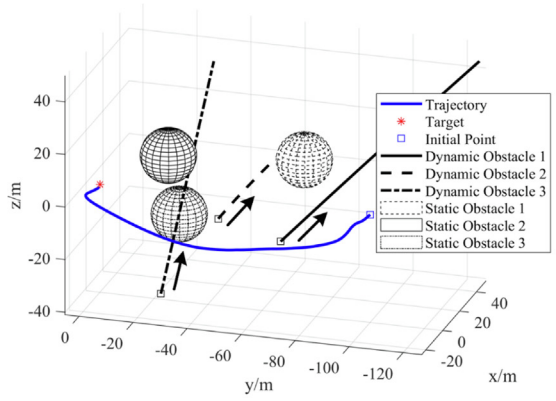

(a) Trajectory of the Servicer

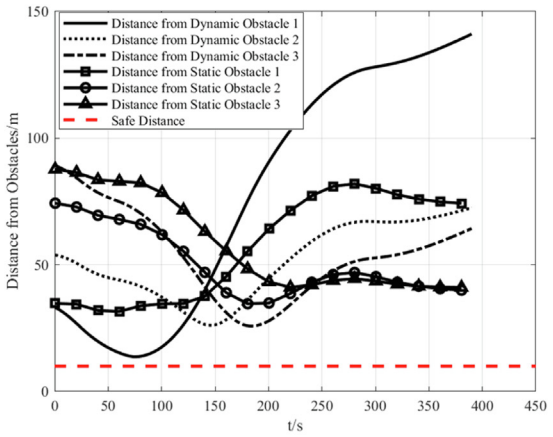

(b) Distance between the Servicer and obstacles

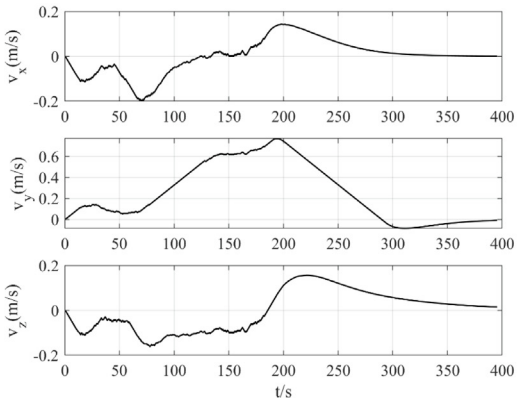

(c) Velocity of the Servicer

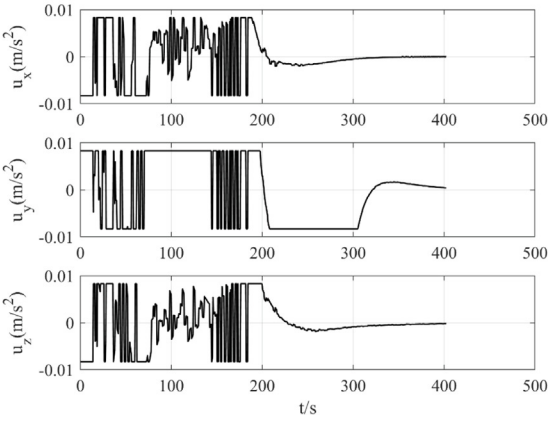

(d) Control acceleration of the Servicer

Fig. 10. Simulation results in Scenario III.

Table 5
The mean and variance of random variables.

Variables	Mean	Variance
The initial position of the Servicer	$[0,-100,0]^T$	$[1,1,1]^T$
The initial position of dynamic Obstacle 1	$[-10,-70,-10]^T$	$[1,1,1]^T$
The initial velocity of dynamic Obstacle 1	$[0.14,\ -0.14,\ 0.14]^T$	$[0.01,0.01,0.01]^T$
The initial position of dynamic Obstacle 2	$[-20,-50,\ 0]^T$	$[1,1,1]^T$
The initial velocity of dynamic Obstacle 2	$[0.18,\ 0,\ 0]^T$	$[0.01,0.01,0.01]^T$
The initial position of dynamic Obstacle 3	$[5,-21,-40]^T$	$[1,1,1]^T$
The initial velocity of dynamic Obstacle 3	$[0,\ -0.05,\ 0.23]^T$	$[0.01,0.01,0.01]^T$
The initial position of static Obstacle 1	$[15,\ -71,\ -12]^T$	$[1,1,1]^T$
The initial position of static Obstacle 3	$[-15,\ -30,\ 20]^T$	$[1,1,1]^T$
The initial position of static Obstacle 3	$[10,\ -20,\ -20]^T$	$[1,1,1]^T$

in the previous section after adding static obstacles, which is the result of the additional repulsion force generated by the static obstacles. Fig. 10 (b) depicts the distance between the Servicer and each obstacle in the process of maneuvering and the closest distance between the Servicer and the obstacle is greater than the safe distance of 10 m, which means the trajectory of the Servicer is outside the forbidden area around the obstacle. Fig. 10(c) shows the curves of velocity over time, indicating that the velocity of the Servicer converges to zero when rendezvousing with the target. In addition, the resulted control signals are given in Fig. 10 (d), which indicates the thrust limitations are satisfied. Finally, the combination of the two potential functions can drive the Servicer flexibly to avoid obstacles, and

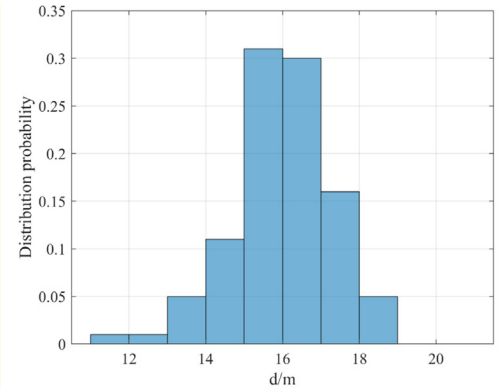

(a) The closest distance between the Servicer and the dynamic Obstacle 1

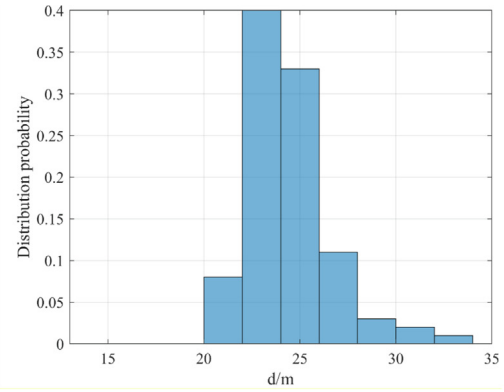

(b) The closest distance between the Servicer and the dynamic Obstacle 2

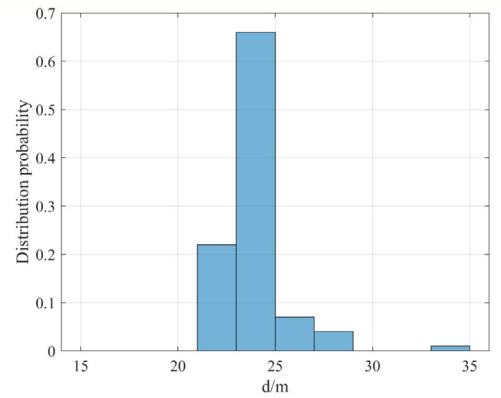

(c) The closest distance between the Servicer and the dynamic Obstacle 2

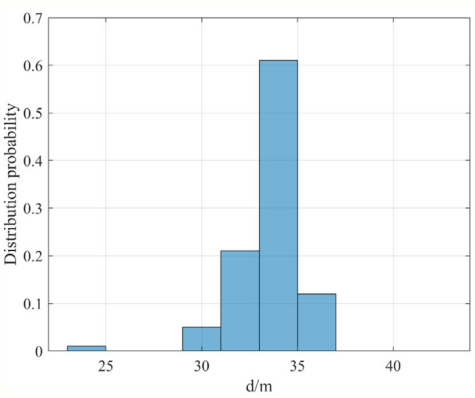

(d) The closest distance between the Servicer and the static Obstacle 1

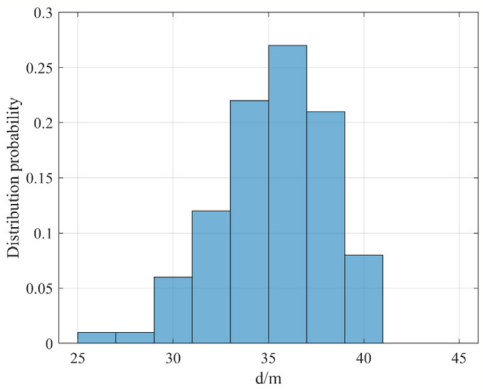

(e) The closest distance between the Servicer and the static Obstacle 2

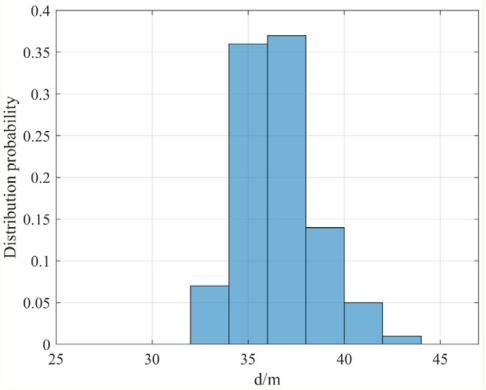

(f) The closest distance between the Servicer and the static Obstacle 3

Fig. 11.

always keep the Servicer stay at a safe distance from obstacles in complex environment.

4.3.1. Monte Carlo simulation

In the simulation of compound space environment, only one condition is considered. Here, a Monte Carlo simulation with a sufficiently high number of realizations is provided to assess whether the proposed control law performs correctly in different scenarios. In the Monte Carlo simulation, the initial configuration is randomly selected from variables that follow a normal distribution. The parameters affecting the simulation results mainly include the initial position of the Servicer, initial position and velocity of the dynamic obstacle, and initial position of the static obstacle. These parameters are chosen as random variables, and they are normally distributed, its mean and variance are shown in Table 5.

We randomly select 100 groups of initial configurations and simulate with the proposed control law. Accordingly, 100 groups of simulation results will be generated. As shown in Fig. 11, the statistical distribution of the proposed control law performance is obtained by statistical processing of 100 groups of results. Fig. 11 plots the statistical distribution of the closest distance between obstacle and Servicer, where results all obey the normal distribution. More importantly, the closest distance to the obstacle in all results is greater than the safe distance of 10 m, indicating correctness and stability of the proposed control law.

Based on the simulation results of the above three scenarios, it can be verified that the designed control law based on the proposed potential functions can realize flexible obstacle avoidance and approach target.

5. Conclusions

This paper mainly studies the autonomous maneuver strategies in the mission of large debris removal based on potential function in the presence of external perturbation, safety constrains, and thrust limitation. Considering the static and dynamic obstacles relative to the target, the potential functions for static obstacles are constructed firstly which can describe the magnitude and range of potential field. Then, the relative velocities of obstacles and the Servicer are introduced to construct potential function for dynamic obstacles, also, the control law is designed based on the gradient of the potential function. The proposed control law is implemented in three scenarios for the Servicer collision avoidance. These scenarios show that the proposed two potential functions can be utilized to implement the Servicer's autonomous avoidance of different types of obstacles when approaching the target debris. In Scenario II, the proposed potential function control law is compared with the SMC-APF control law, which proves the proposed algorithm has better performance. In Scenario III, analysis of Monte Carlo simulation is carried out, which indicates the validity of the proposed algorithm from the perspective of statistical analysis. Through autonomous obstacle avoidance strategy, the Servicer can safely approach the target, and de-orbit the debris to purify the space environment. In the future, the optimal control problem of the potential function will be considered, optimization methods such as neural networks, can be used to optimize the parameters of potential function.

Declaration of Competing Interest

The authors declare that they have no known competing financial interests or personal relationships that could have appeared to influence the work reported in this paper.

Acknowledgements

This research was funded by the "National Natural Science Foundation of China", grant number 51905272.

References

Aglietti, G.S., Taylor, B., Fellowes, S., et al., 2020. The active space debris removal mission RemoveDebris. Part 2: in orbit operations. Acta Astronaut. 168, 310–322.

Badawy, A., McInnes, C.R., 2008. On-orbit assembly using superquadric potential fields. J. Guidance, Control Dynamics 31 (1), 30–43.

Bowen, J., Villa, M., Williams, A., 2015. Cubesat based rendezvous, proximity operations, and docking in the CPOD mission. 29th Annual AIAA/USU Conference on Small Satellites.

Cao, L., Qiao, D., Xu, J., 2018. Suboptimal artificial potential function sliding mode control for spacecraft rendezvous with obstacle avoidance. Acta Astronaut. 143, 133–146.

Choi, D., Chhabra, A., Kim, D., 2021. Intelligent cooperative collision avoidance via fuzzy potential fields. Robotica 2021, 1–20.

Forshaw, J.L., Aglietti, G.S., Fellowes, S., et al., 2020. The active space debris removal mission RemoveDebris. Part 1: from concept to launch. Acta Astronaut. 168, 293–309.

Friudenberg, P., Koziol, S., 2018. Mobile robot rendezvous using potential fields combined with parallel navigation. IEEE Access 6, 16948–16957.

Ge, S.S., Cui, Y.J., 2002. Dynamic motion planning for mobile robots using potential field method. Autonomous robots 13, 207–222.

Hu, D., Pang, B., Chi, R., et al., 2021. Survivability assessment of spacecraft impacted by orbit debris. Defence Technology 17, 961–970.

Jiang C, Yang B, Cao L, et al. 2021. Interfered Fluid Dynamical Controller for Spacecraft Rendezvous with Collision-Free. 2021 IEEE 7th International Conference on Control Science and Systems Engineering. IEEE, 2021, 88-92.

Kessler DJ, Johnson NL, Liou JC, et al. 2010. The kessler syndrome: implications to future space operations. Advances in the Astronautical Sciences, 137, AAS 10-016.

Khatib, O., 1986. Real-time obstacle avoidance for manipulators and mobile robots. Autonomous robot vehicles 1986, 396–404.

Letizia, F., Colombo, C., Lewis, H.G., 2016. Collision probability due to space debris clouds through a continuum approach. J. Guidance, Control Dynamics 39, 2240–2249.

Liou, J.C., 2008. A statistical analysis of the future debris environment. Acta Astronaut. 62, 264–271.

Liou, J.C., 2011. An active debris removal parametric study for LEO environment remediation. Adv. Space Res. 47, 1865–1876.

Li, Q., Zhang, B., Yuan, J., et al., 2018. Potential function based robust safety control for spacecraft rendezvous and proximity operations under path constraint. Adv. Space Res. 62, 2586–2598.

Lopez, I., Mclnnes, C.R., 1995. Autonomous rendezvous using artificial potential function guidance. J. Guidance, Control Dynamics 18, 237–241.

Mancini, M., Bloise, N., Capello, E., Punta, E., 2019. Sliding mode control techniques and artificial potential field for dynamic collision avoidance in rendezvous maneuvers. IEEE Control Systems Letters 4 (2), 313–318.

Mark, C.P., Kamath, S., 2019. Review of active space debris removal methods. Space Policy 47, 194–206.

Munoz, J.D., 2011. Rapid path-planning algorithms for autonomous proximity operations of satellites. University of Florida.

Nanjangud, A., Blacker PC,Bandyopadhyay S,, et al., 2018. Robotics and AI-enabled on-orbit operations with future generation of small satellites. Proc. IEEE 106, 429–439.

Naumann KW, Weigand A, Ringeisen A. 2019. Solid rocket motors for the de-orbiting of satellites. 8th European conference for aeronautics and space sciences, Madrid.

Nishida, S.I., Kawamoto, S., Okawa, Y., et al., 2009. Space debris removal system using a small satellite. Acta Astronaut. 65, 95–102.

Omri, K., Pini, G., 2021. Spacecraft relative navigation with an omnidirectional vision sensor. Acta Astronaut. 2021 (188), 334–351.

Pang, B.J., Wang, D.F., Xiao, W.K., Peng, K.K., 2015. The influence of US satellite DMSP-F13 breakup event on space debris environment. Spacecraft Environment Eng. 32, 349–356.

Patle, B.K., Pandey, A., Parhi, D.R.K., et al., 2019. A review: On path planning strategies for navigation of mobile robot. Defence Technology 15, 582–606.

Pongvthithum, R., Veres, S.M., Gabriel, S.B., et al., 2005. Universal adaptive control of satellite formation flying. Int. J. Control 78, 45–52.

Prahlad V, Kay CD, Wang ML. 2000. Evolutionary artificial potential fields and their application in real time robot path planning. Proceedings of the 2000 congress on evolutionary computation. IEEE, 2000(1), 256-263.

Prevost, C.G., Desbiens, A., Gagnon, E., 2007. Extended Kalman Filter for State Estimation and Trajectory Prediction of a Moving Object Detected by an Unmanned Aerial Vehicle, 2007 American Control Conference. IEEE 2007, 1805–1810.

Roberto, O., Alessia, N., 2019. Uncooperative spacecraft relative navigation with LIDAR-based unscented Kalman filter. IEEE Access 2019 (7), 180012–180026.

Roger, A.B., McInnes, C.R., 2000. Safety constrained free-flyer path planning at the international space station. J. Guidance, Control Dynamics 23, 971–979.

Salnikova, T., Stepanov, S., Kugushev, E., 2020. Interaction of compact space debris clouds. Acta Astronaut. 176, 613–619.

Shan, M., Guo, J., Gill, E., 2020. An analysis of the flexibility modeling of a net for space debris removal. Adv. Space Res. 65, 1083–1094.

Sun, H.Q., Zhang, Z.Y.Z., Hu, E.W., 2020. Comparative Research on Early Warning Determination Methods of Spacecraft Collision. IOP Conference Series: Materials Science and Engineering. IOP Publishing 751, 12–18.

Valencia S, Eng B. 2021. Analyses of the Russian antisatellite ASAT missile test on Kosmos-1408 and its impact on space sustainability. https://www.researchgate.net/ publication/356379465.

Van der Ha, J., Mugellesi, R., 1990. Analytical models for relative motion under constant thrust. J. Guidance, Control, Dynamics 13 (4), 644–650.

Yang, X., Zong, Q., Zhang, X., et al., 2022. Adaptive Finite-Time Reconfiguration Control for Spacecraft Formation with Collision Avoidance. Adv. Guidance, Navigation Control 2022, 1961–1971.

Yu, Y., Yue, C., Li, H., et al., 2021. Autonomous Low-Thrust Control of Long-Distance Satellite Clusters Using Artificial Potential Function. J. Astronautical Sciences 68, 71–95.

Zhang, J.R., Zhao, S.G., Zhang, Y., 2015. Autonomous guidance for rendezvous phasing based on special-point-based maneuvers. J. Guidance, Control Dynamics 38, 578–586.

Zhu, S., Yang, H., Cui, P., et al., 2022. Anti-collision zone division based hazard avoidance guidance for asteroid landing with constant thrust. Acta Astronaut. 190, 377–387.